

## STRAIN GRADIENT PLASTICITY: THEORY AND EXPERIMENT

N. A. FLECK<sup>1</sup>, G. M. MULLER<sup>1</sup>, M. F. ASHBY<sup>1</sup> and J. W. HUTCHINSON<sup>2</sup>

<sup>1</sup>Cambridge University Engineering Department, Trumpington Street, Cambridge CB2 1PZ, England and

<sup>2</sup>Division of Applied Sciences, Harvard University, Oxford Street, Cambridge, MA 02138, U.S.A.

(Received 5 March 1993; in revised form 24 June 1993)

**Abstract**—Dislocation theory is used to invoke a strain gradient theory of rate independent plasticity. Hardening is assumed to result from the accumulation of both randomly stored and geometrically necessary dislocations. The density of the geometrically necessary dislocations scales with the gradient of plastic strain. A deformation theory of plasticity is introduced to represent in a phenomenological manner the relative roles of strain hardening and strain gradient hardening. The theory is a non-linear generalization of Cosserat couple stress theory. Tension and torsion experiments on thin copper wires confirm the presence of strain gradient hardening. The experiments are interpreted in the light of the new theory.

### 1. INTRODUCTION

#### 1.1. Scale effects in plasticity

In this paper we develop a phenomenological plasticity law which accounts for a size dependence on strength. In conventional plasticity theory no length scale enters the constitutive law and no size effects are predicted. However, several observed plasticity phenomena display a size effect whereby the smaller is the size the stronger is the response. As examples: the indentation hardness of metals and ceramics increases as the size of the indenter is decreased [1]; the strengthening of metals by a given volume fraction of hard particles is greater for small particles than for large, for the same volume fraction of reinforcement, as is their rate of work hardening [2, 3]; and fine-grained metals are stronger than those with coarse grains [4]. The effect becomes pronounced when the indent size, grain size or particle spacing lies below approximately 10  $\mu\text{m}$ .

These effects may not all have the same explanation, but it is clear that all require a length scale for their interpretation. A natural way to include size effects in the constitutive law is to postulate that the yield stress depends both upon strain and strain gradient. We adopt this approach in the current paper, and provide evidence for the strengthening due to a strain gradient by experiments on the tension and torsion responses of thin copper wires. In tension the strain is uniform and no size dependence of strength is observed. In torsion, however, the thinner is the wire the greater is the gradient of strain for a given surface shear strain, and the stronger is the response.

Conventional plasticity theories, as we have said, possess no internal length scale. When the length scale associated with the deformation field is large, strain gradients are small and conventional theories

suffice. On the other hand, when the length scale associated with the deformation field is small compared to a material length scale explained below, it becomes necessary to include the strain gradient term in the constitutive law. The purpose of this paper is to present a plasticity theory which includes an internal material length scale, and to provide supporting experimental evidence. The underlying idea is that material hardening is controlled by the total density of dislocations, part of which derives from, and is directly proportional to, the gradient of strain. The distinction between dislocations stored during uniform straining and those necessitated by gradients of strain can be understood as follows.

When a plastic crystal is deformed, dislocations are generated, move, and are stored; the storage causes the material to work harden. Dislocations become stored for two reasons: they accumulate by trapping each other in a random way or they are required for compatible deformation of various parts of the crystal. The dislocations which trap each other randomly are referred to as *statistically stored dislocations* [5, 6]. As yet, there is no simple argument to estimate the density  $\rho_s$  of these dislocations, although it has been measured, as a function of strain, by numerous investigators.

Gradients of plastic shear result in the storage of *geometrically necessary dislocations* [5–8]. Plastic strain gradients appear either because of the geometry of loading or because the material itself is plastically inhomogeneous (containing non-deforming phases, for instance). As examples: in the plastic twisting of a cylinder or bending of a beam, the strain is finite at the surface but zero along the axis of twist or of bending [Fig. 1(a, b)]; in the hardness test the strain is large immediately beneath the indenter but zero far from it; and in the plastic zone at the tip of

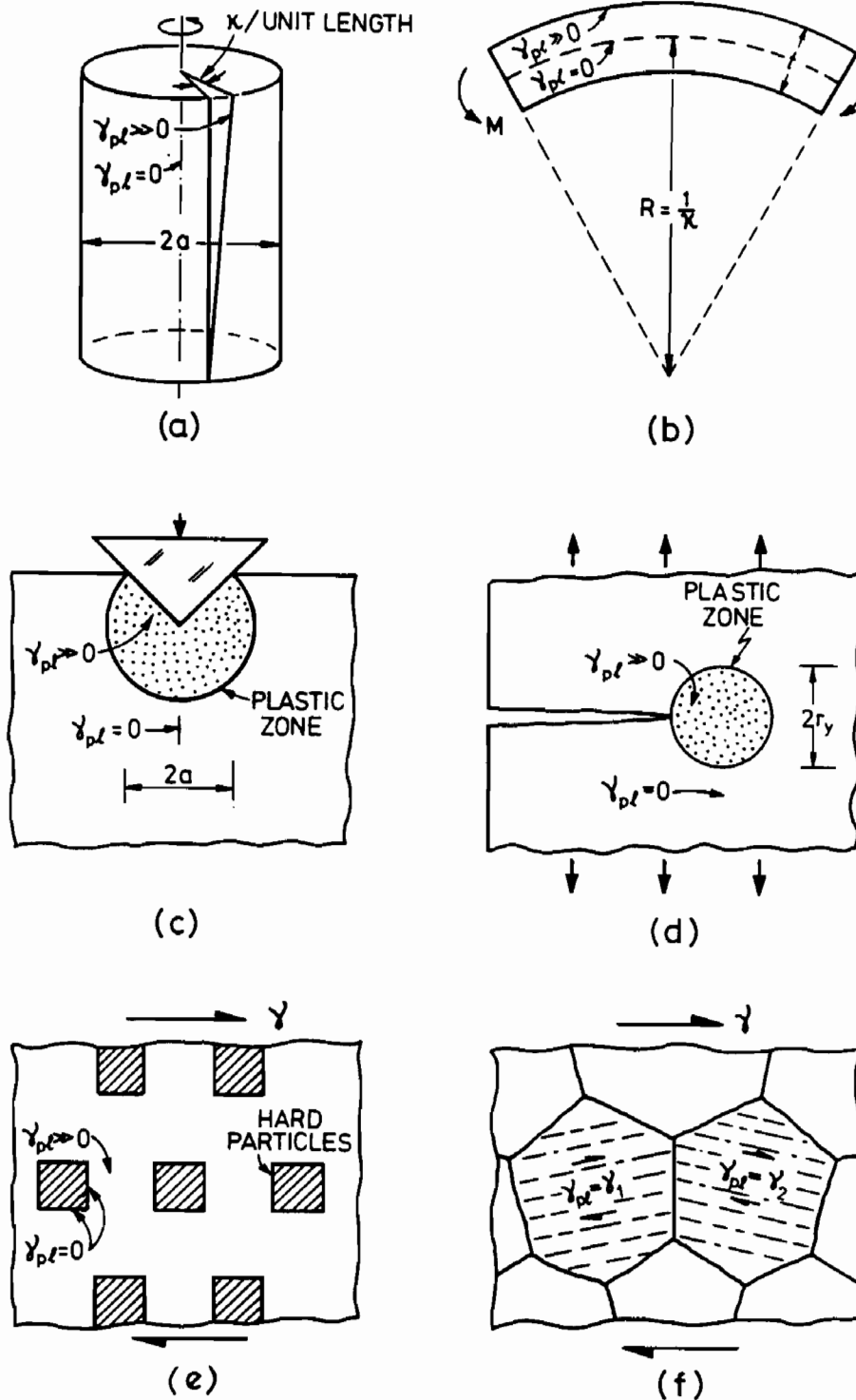


Fig. 1. Plastic strain gradients are caused by the geometry of deformation (a, b), by local boundary conditions (c, d) or by the microstructure itself (e, f).

a crack in an otherwise elastic medium steep gradients of plastic strain appear [Fig. 1(c, d)]; in the deformation of plastic crystals containing hard, non-deforming particles local strain gradients are generated between particles; and in the plastic deformation of polycrystals, the mismatch of slip at the bound-

aries of the grains can induce gradients of plastic strain there [Fig. 1(e, f)]. In approximate terms, the magnitude of the plastic strain gradient is of the order of the average shear strain in the crystal divided by the local length scale  $\lambda$  of the deformation field. These strain gradients require, for compatibility reasons,

the presence of geometrically necessary dislocations of density  $\rho_G$ , where [5]

$$\rho_G \approx \frac{4\gamma}{b\lambda}. \quad (1.1)$$

Here,  $\gamma$  is the macroscopic plastic shear strain and  $b$  is the magnitude of the Burger's vector  $\mathbf{b}$ . The geometrically necessary dislocations contribute to hardening and, in the limit that  $\rho_G \gg \rho_S$ , the macroscopic shear yield stress  $\tau$  can be written approximately as

$$\tau \approx C'Gb\sqrt{\rho_G} \quad (1.2)$$

where  $G$  is the shear modulus and  $C'$  is a constant of order unity. In the torsion test,  $\lambda$  is simply the radius of the cylinder; in bending it is the half thickness of the beam; in the hardness test it is related to the indent size; at the crack tip, to the plastic zone size; and in metals containing non-deforming particles  $\lambda$  is related to the particle separation, approximately  $r/f$ , where  $r$  is the radius and  $f$  is the volume fraction of the particles. In polycrystals one might expect it to be related to the grain size.

Direct support for the notion that geometrically necessary dislocations lead to enhanced hardening comes from the compression tests of Russell and Ashby [9], Brown and Stobbs [10] and many others. Here the plate-like  $\theta'$  precipitates lead to the storage of geometrically necessary dislocations and the appearance of lattice curvature, in good agreement with equation (1.1); and the enhancement in flow stress scales as the square root of  $\rho_G$ , as suggested by equation (1.2). The well known size effect in hardness has recently been given a quantitative interpretation in terms of geometrically necessary dislocations by Brown [1]. Experimental data [4] confirm that fine grained metals work harden faster than coarse grained metals.

Conventional plasticity laws tacitly assume that  $\rho_G \ll \rho_S$  and no length scale enters. Figure 2 shows a comparison of  $\rho_G$  and  $\rho_S$  as a function of shear strain  $\gamma$  for a variety of microstructural length scales  $\lambda$  for pure copper. The shaded band marked "Single Crystal" is the measured density  $\rho_S$  of statistically stored dislocations in single crystal copper, oriented for (initial) easy glide; it is derived from the measurements of Basinski and Basinski [11]. There are three stages. In stage I, slip is on one system only, dislocations trap as dipoles and dislocation storage is proportional to strain; in the second stage, slips are induced on secondary systems and the storage becomes proportional to the square of the strain; and in the final, third, stage, recovery mechanisms such as cross-slip deplete the dislocation population, reducing the rate of storage once more. In polycrystals, stages I and II are absent, and the storage rate is at first rapid, decreasing to an almost linear increase with strain (corresponding to parabolic hardening,  $\sigma \propto \epsilon^{0.5}$ ) above a strain of a few percent, as

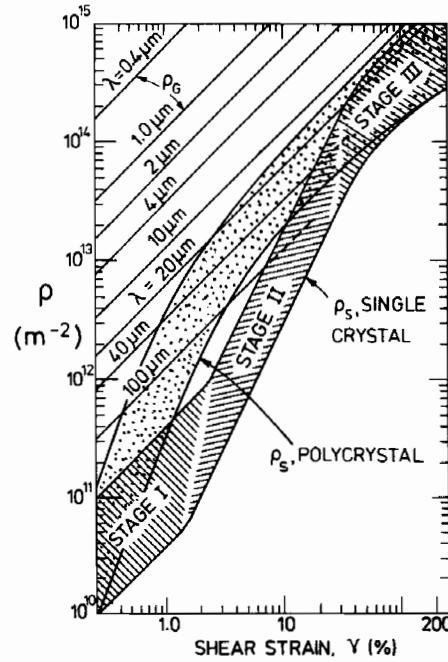


Fig. 2. The density of statistically stored dislocations  $\rho_S$ , and geometrically necessary dislocations  $\rho_G$  plotted against shear strain. The single crystal density  $\rho_S$  (shaded band) is taken from the experimental data of Basinski and Basinski [11]; that for polycrystals is inferred from stress-strain curves. The density  $\rho_G$  is shown as a set of parallel lines for assumed values of microstructural length scale  $\lambda$ , using equation (1.1).

shown in the shaded band labeled "Polycrystal". It is to be emphasized that these are the densities of dislocations which characterize deformation which is *macroscopically uniform*: that is, one in which no gradients of strain are imposed. When gradients are present, additional dislocations are required to accommodate them. The figure shows this contribution, calculated from equation (1.1) for various length scales  $\lambda$  set, as explained, by the particular aspect of geometry (wire radius or beam thickness), imposed displacements (the hardness test) or microstructural feature (particles or grain boundaries) which induce them. We note that at 10% strain  $\rho_G \gg \rho_S$  for  $\lambda < 50 \mu\text{m}$  in single crystals and for  $\lambda < 20 \mu\text{m}$  in polycrystals. Thus, there is a regime where the density of geometrically necessary dislocations swamp the statistically stored ones and hardening is strongly dependent upon strain gradient effects. The smaller the length scale of the gradients, the more important the effects become.

The main emphasis of the present paper is to develop a continuum theory of plasticity which captures the transition from behavior which is independent of strain gradients to that dominated by strain gradient effects. There have been previous attempts to include strain gradients within a plasticity formulation, notably those of Aifantis [12], Muhlhaus and Aifantis [13, 14] and Zbib and Aifantis [15]. One application these authors have in mind is to bring in

a length scale associated with localization phenomena. The theories proposed until now have not involved geometrically necessary dislocations, but are mainly based upon ideas on the thermally activated diffusion of dislocations under a potential gradient.

In order to motivate the full 3D theory of geometrically necessary dislocations we use physical arguments to deduce the density of geometrically necessary dislocations in a beam subjected to non-uniform shear.

1.2. Non-uniform shear of a beam

Consider a beam made from a single crystal and aligned with the Cartesian axes  $(x_1, x_2, x_3)$ , as shown in Fig. 3. Assume that the beam suffers non-uniform shear, such that the displacement field is

$$u_1 = 0, \quad u_2 = \frac{1}{2} \kappa x_1^2, \quad u_3 = 0 \quad (1.3)$$

where the ‘‘curvature’’  $\kappa$  is a constant. Further, neglect elastic straining and assume that this displacement field is achieved by a combination of plastic slip  $\gamma$  on a single slip system, and lattice rotation. The relative proportion of slip and lattice rotation depends upon the orientation of the slip system. For the case where the normal to the slip plane  $\mathbf{m}$  is aligned with the  $x_1$  direction and the slip direction  $\mathbf{s}$  is in the  $x_2$  direction, the displacement field is achieved by a slip distribution  $\gamma(x_1, x_2) = \kappa x_1$  accompanied by zero rotation of the lattice, see Fig. 3. In the language of dislocation theory, no storage of dislocations is required since the displacements can be achieved by the passage of dislocations from one surface to the other.

Alternatively, consider the case where the normal to the slip plane  $\mathbf{m}$  is parallel to the  $x_2$  direction and the slip direction  $\mathbf{s}$  is along the  $x_1$  direction, as shown in Fig. 4(a). The displacement field (1.3) may be rewritten

$$u_1 = -\kappa x_1 x_2 + \kappa x_1 x_2 = 0 \quad (1.4a)$$

$$u_2 = \frac{1}{2} \kappa x_1^2 \quad (1.4b)$$

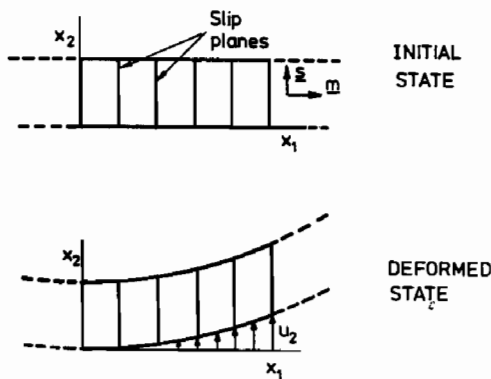


Fig. 3. A beam subjected to non-uniform shear. Plastic slip is assumed to occur on a single slip system with unit normal  $\mathbf{m}$  aligned with the  $x_1$  axis, and slip direction  $\mathbf{s}$  aligned with the  $x_2$  axis.

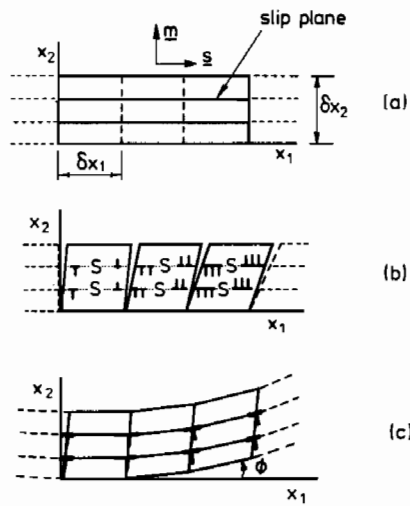


Fig. 4. Sketch showing that a gradient of slip in the  $x_1$  direction causes a density  $\rho_G$  of geometrically necessary dislocations to be stored. Plastic slip is assumed to occur on a single slip system with unit normal  $\mathbf{m}$  aligned with the  $x_2$  axis, and slip direction  $\mathbf{s}$  aligned with the  $x_1$  axis.

and

$$u_3 = 0 \quad (1.4c)$$

where the particular choice of trivial decomposition in (1.4a) will become apparent shortly. The term  $(-\kappa x_1 x_2)$  in (1.4a) and the term  $(\frac{1}{2} \kappa x_1^2)$  in (1.4b) may be interpreted as the displacement field associated with a lattice rotation  $\phi$  of  $\kappa x_1$ ; the axis of rotation is along the  $x_3$  direction. The remaining term  $(\kappa x_1 x_2)$  in (1.4a) is due to plastic slip on the assumed single slip system; thus  $\gamma = \kappa x_1$ . That this slip distribution requires the storage of geometrically necessary dislocations can be seen as follows. Start from the assumption that the shear strain due to slip on the slip system depicted in Fig. 4(a) is given by  $\gamma = \kappa x_1$ ; a compatibility argument is used to calculate the density of dislocations  $\rho_G$  and the displacement field (1.3).

Divide the crystal up into small rectangular cells of side  $\delta x_1, \delta x_2$ , three of which are shown in Fig. 4(a). A gradient of shear deforms the cells by different amounts. If they were not stuck together they would appear as shown in Fig. 4(b), and the displacement field  $u_i$  would be discontinuous or *incompatible*. Imagine that a shear strain  $\gamma$  in each cell is produced by generating dipoles of Burger’s vector  $\mathbf{b}$  within each cell, and by allowing the dipoles to expand outward to the surfaces as shown in Fig. 4(b). The number of such dipoles  $n$  in a cell is given by a Burger’s circuit construction as

$$nb = \gamma \delta x_2 \quad (1.5)$$

where  $b$  is the magnitude of  $\mathbf{b}$ . (We assume that  $n$  is large, although only a small number of dislocations are shown in Fig. 4 for the sake of clarity.) Now rejoin the cells, allowing cancellation of the positive

dislocations at the surface of one cell with the negative ones of the neighboring cell, see Fig. 4(c). An excess  $\Delta n$  of dislocations is left at each cell wall, given by

$$\Delta n b = \delta \gamma \delta x_2 = \frac{\partial \gamma}{\partial x_1} \delta x_1 \delta x_2. \quad (1.6)$$

Thus a density of geometrically necessary dislocations  $\rho_G$  of

$$\rho_G = \frac{1}{b} \frac{\partial \gamma}{\partial x_1} \quad (1.7)$$

is stored on the single slip system. Since  $\gamma = \kappa x_1$  the density of dislocations is  $\rho_G = \kappa/b$  via (1.7). An additional rotation of the lattice is required in order to ensure that gaps do not develop. Each cell is rotated by an amount  $\delta \phi = \delta \gamma = \rho_G b \delta x_1$  by (1.6). Thus the lattice adopts a curvature  $K = \delta \phi / \delta x_1$  given by

$$K = \rho_G b = \kappa. \quad (1.8)$$

The displacement field (1.3) follows immediately.

The above examples illustrate several inherent features of geometrically necessary dislocations. They are associated with gradients of slip and their density can be calculated directly by geometry, once the active slip systems have been defined. The same displacement field may or may not give rise to geometrically necessary dislocations, depending upon the distribution of active slip systems. Lattice rotation (and elastic stretching of the lattice) is usually needed in order to ensure compatibility of displacement.

## 2. TORSION EXPERIMENTS ON COPPER WIRES

In order to obtain direct experimental evidence for strain gradient hardening, the tensile and torsional responses were measured for polycrystalline copper wires (99.99% purity) ranging in diameter from 12 to 170  $\mu\text{m}$ . In uniaxial tension strain gradients are negligible and hardening is due to the accumulation of statistically stored dislocations. In torsion of a circular wire the shear strain  $\gamma$  varies with radius  $r$  from the axis of twist, such that  $\gamma = \kappa r$ , where  $\kappa$  is the twist per unit length of the wire. The strain gradient  $d\gamma/dr = \kappa$  induces a density  $\rho_G$  of geometrically necessary dislocations of order  $\kappa/b$ . Thus the wire is hardened by both statistically stored and geometrically necessary dislocations. For a given shear strain at the surface of the wire (or, equivalently, for a given average strain across the section) the thinner wire has the greater strain gradient  $d\gamma/dr$  and the higher density of geometrically necessary dislocations. We therefore expect faster work hardening in the thinner wire. The experiments reported below confirm this expectation.

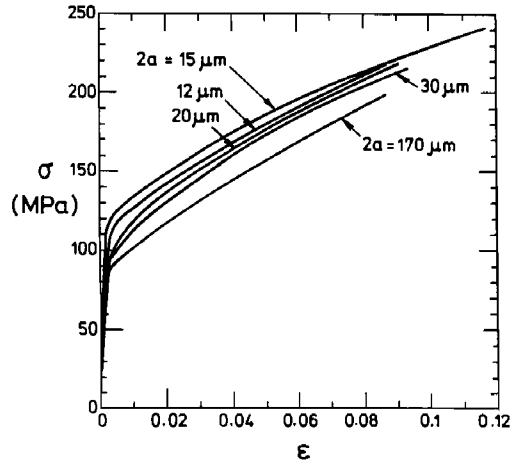


Fig. 5. True stress  $\sigma$  vs logarithmic strain  $\epsilon$  tension data for copper wires of diameter  $2a$  in the range 12–170  $\mu\text{m}$ . There is a negligible effect of wire diameter on the behavior.

### 2.1. Test method

Tension and torsion test were performed on commercially pure, cold drawn copper wires of diameter in the range 12 to 170  $\mu\text{m}$ . All the wires were annealed, giving grain sizes between 5 and 25  $\mu\text{m}$ , the larger diameter wires having the larger grain sizes. The tension tests were performed at a strain rate of  $10^{-3} \text{ s}^{-1}$ , and the torsion tests were performed such that the shear strain rate at the surface of the wire  $\dot{\gamma}$  was also  $10^{-3} \text{ s}^{-1}$ . Details of the test method and apparatus are given in Appendix A.

### 2.2. Experimental results

Uniaxial tension data for the copper wires are shown in Fig. 5 and the torsion response is given in Fig. 6. Typical responses are given for each wire diameter  $2a$ ; generally, we performed at least four tests of each type for each diameter of wire. We conclude from Fig. 5 that there is only a minor influence of wire diameter on tensile behavior. No

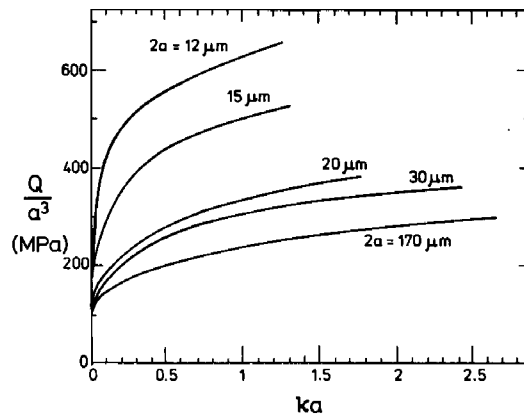


Fig. 6. Torsional response of copper wires of diameter  $2a$  in the range 12–170  $\mu\text{m}$ . If the constitutive law were independent of strain gradients, the plots of normalized torque  $Q/a^3$  vs  $ka$  would all lie on the same curve.

systematic trend between tensile stress-strain curve and diameter emerges for diameters in the range 12 to 30  $\mu\text{m}$ . The data for  $2a = 170 \mu\text{m}$  is approximately 10% below that of the other curves, perhaps because the grain size was significantly larger here than in the other wires.

The torsion data in Fig. 6 have been displayed in the form  $Q/a^3$  vs  $\kappa a$ , where  $Q$  is the torque,  $a$  the wire radius and  $\kappa$  the twist per unit length. The non-dimensional group  $\kappa a$  may be interpreted as the magnitude of the shear strain at the surface of the wire. The group  $Q/a^3$  gives a measure of the shear stress across the section of the wire in some averaged sense. Dimensional analysis establishes the fact that  $Q/a^3$  is a function of  $\kappa a$  but is otherwise independent of  $a$  for any constitutive law which does not contain a length scale. Thus, if the local shear stress at any point in the wire were to depend only upon shear strain and not strain gradient, the curves of  $Q/a^3$  vs  $\kappa a$  would superpose. Plainly they do not. There is a systematic increase in torsional hardening with decreasing wire diameter. For example, at  $\kappa a = 0.3$ , the value of  $Q/a^3$  for  $2a = 12 \mu\text{m}$  is approximately three times the value of  $Q/a^3$  for  $2a = 170 \mu\text{m}$ . This supports the notion that strain gradient strengthening plays an increasingly dominant role with decreasing wire diameter.

A log-log plot of  $Q/a^3$  vs  $\kappa a$  for all diameters of wire is given in Fig. 7. The lines are approximately straight and parallel, and display an average slope of 0.20, indicating a power law relationship,  $Q/a^3 \propto (\kappa a)^N$ , between the variables with a value for the hardening exponent  $N$  of 0.20.

### 3. SINGLE CRYSTAL FORMULATION FOR GEOMETRICALLY NECESSARY DISLOCATIONS

The relationship between plastic strain gradient and dislocation density has been explored by Nye [7]

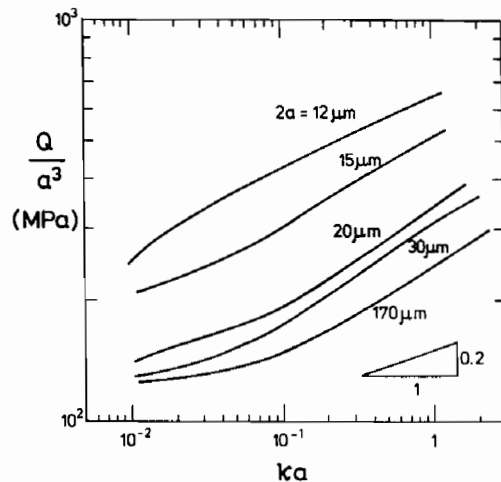


Fig. 7. Logarithmic plot of  $Q/a^3$  vs  $\kappa a$  for the copper wires in torsion.

and Kroner [16–18]. We summarize the theory for the case of small deformations. (A precise framework for formulating elastic-plastic single crystal constitutive relations at finite strains has been laid down by Hill and Rice [19]; the theoretical development given below can be extended to the finite strain regime in a fairly straightforward manner.) It is re-emphasized that the concern is with the characteristics of a distribution of large numbers of dislocations, and not with individual dislocation interactions.

In order to calculate the density of geometrically necessary dislocations, a crystal lattice is embedded within the solid. We assume that the material flows through the crystal lattice by dislocation motion, and that the lattice (and attached material) undergoes rotation and elastic stretching. Consider the relative displacement  $du_i$  of two material points separated by  $dx_j$ , in the Cartesian reference frame of Fig. 8. The relative displacement  $du_i$  is decomposed into

$$du_i = du_i^S + du_i^R + du_i^E \quad (3.1a)$$

where

$$du_i^S \equiv \gamma_{ij} dx_j \quad (3.1b)$$

$$du_i^R \equiv \phi_{ij} dx_j \quad (3.1c)$$

and

$$du_i^E = \epsilon_{ij}^E dx_j. \quad (3.1d)$$

Here,  $du_i^S$  is the relative displacement due to slip,  $du_i^R$  is due to lattice rotation and  $du_i^E$  is due to elastic stretching of the lattice;  $du_i^S$  is linearly related to  $dx_j$  via the slip tensor  $\gamma_{ij}$ ,  $du_i^R$  is related to  $dx_j$  via the rotation tensor  $\phi_{ij}$ , and  $du_i^E$  is related to  $dx_j$  via the elastic strain tensor  $\epsilon_{ij}^E$ .

A particular slip system,  $\alpha$ , is specified by the vectors  $(\mathbf{s}^{(\alpha)}, \mathbf{m}^{(\alpha)})$  where  $\mathbf{s}^{(\alpha)}$  is the slip direction and  $\mathbf{m}^{(\alpha)}$  is the slip plane normal. The slip tensor  $\gamma_{ij}$  is associated with an amount of slip  $\gamma^{(\alpha)}$  on each of the active slip systems, hence

$$\gamma_{ij} = \sum_{\alpha} \gamma^{(\alpha)} s_i^{(\alpha)} m_j^{(\alpha)} \quad (3.2)$$

where the summation is taken over all active slip systems.

The density of geometrically necessary dislocations is related to the net Burger's vector  $B_i$  associated with crystallographic slip. Make a cut in the crystal in

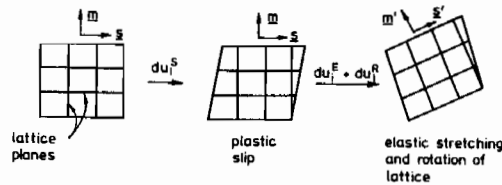


Fig. 8. The elastic-plastic deformation of a single crystal. Here,  $du_i^S$  is illustrated for single slip while in the text  $du_i^S$  is defined for the general case of multi-slip.

order to produce a surface  $S$  of outward normal  $\mathbf{n}$ . Define  $B_i$  as the resulting displacement on completion of a Burger's circuit around the periphery  $\Gamma$  of the surface  $S$ . In other words,  $B_i$  completes the circuit when  $\Gamma$  is traversed in the sense of a right-handed screw motion along  $\mathbf{n}$ . Thus,  $B_i$  is

$$B_i = \oint_{\Gamma} du_i^S = \oint_{\Gamma} \gamma_{ij} dx_j \quad (3.3)$$

which may be rewritten using Stokes' theorem as

$$B_i = \int_S \alpha_{in} n_n dS \quad (3.4)$$

where

$$\alpha_{in} = e_{nkj} \gamma_{ijk}. \quad (3.5)$$

In (3.5)  $e_{nkj}$  denotes the alternating tensor. The tensor  $\alpha$  is Nye's *dislocation density tensor* or torsion-flexure tensor and gives a direct measure of the number of geometrically necessary dislocations. Kroner's  $\alpha$  tensor, here labeled  $\alpha_K$ , is related to Nye's tensor  $\alpha$  by  $\alpha_K = -\alpha^T$ , where the superscript T denotes the transpose. Nye [7] has related  $\alpha$  to the distribution of individual dislocations within a crystal as follows. Suppose there exist dislocations with length parallel to the unit vector  $\mathbf{r}$  and with Burger's vector  $\mathbf{b}$ . Let there be  $N$  of these dislocations crossing unit area normal to  $\mathbf{r}$ . The number crossing a unit area normal to the unit vector  $\mathbf{n}$  is  $N\mathbf{n} \cdot \mathbf{r}$ , and the associated Burger's vector is  $N(\mathbf{n} \cdot \mathbf{r})\mathbf{b}$ . Hence in suffix notation  $B_i = Nn_j r_j b_i$  and from (3.4)

$$\alpha_{ij} = Nb_i r_j. \quad (3.6)$$

If there are other sets of dislocations present with different values of  $N$ ,  $\mathbf{b}$  and  $\mathbf{r}$ , then the total  $\alpha_{ij}$  is obtained by summing the values of  $Nb_i r_j$  from each set.

We emphasize that the net displacement  $\oint du_i$  vanishes along any closed path within the material, and that the incompatibility in displacement  $B_i = \oint du_i^S$  is exactly matched by an equal and opposite displacement mismatch  $\oint (du_i^R + du_i^E)$ , as demanded by (3.1a). It is clear from (3.1a) and (3.4–3.6) that the density of geometrically necessary dislocations is defined unambiguously only when a crystal structure is embedded in the material. We treat  $\alpha_{ij}$  as the fundamental measure of the total density of geometrically necessary dislocations.

An alternative version of the expression (3.5) for  $\alpha_{ij}$  may be derived through introduction of the unit vector  $\mathbf{t} \equiv \mathbf{s} \times \mathbf{m}$ . Note that  $(\mathbf{s}, \mathbf{m}, \mathbf{t})$  forms a right-handed triad with  $\mathbf{t}$  in the slip plane and orthogonal to  $\mathbf{s}$ . Substitution of the relation  $\mathbf{m} = \mathbf{t} \times \mathbf{s}$  in (3.2) gives via (3.5)

$$\alpha_{in} = \sum_{\alpha} s_i^{(\alpha)} \gamma_{jk}^{(\alpha)} (s_k^{(\alpha)} t_n^{(\alpha)} - t_k^{(\alpha)} s_n^{(\alpha)}). \quad (3.7)$$

The dependence of  $\alpha$  upon the slip gradient in the slip direction  $\mathbf{s}$ , and in the transverse direction  $\mathbf{t}$ , is made explicit by (3.7). Note that a slip gradient in the  $\mathbf{m}$

direction does not contribute to  $\alpha$ , as illustrated in Fig. 3.

#### 4. PRELIMINARIES IN THE DEVELOPMENT OF A PHENOMENOLOGICAL CONSTITUTIVE LAW FOR STRAIN GRADIENTS

In the following sections a generalization of classical  $J_2$ -deformation theory will be developed in order to include strain gradient effects. Just as in the classical theory, the strain gradient deformation theory is limited to applications where loading is proportional or close to proportional. We motivate the theory by first considering the nature of the constitutive law for slip on a single system.

##### 4.1. Slip on a single system

Consider slip on a single system of a single crystal, and assume that hardening is governed by the sum of the densities of statistically stored dislocations,  $\rho_S$ , and geometrically necessary dislocations,  $\rho_G$ . The simplest possible dimensionally correct relationship between flow stress  $\tau$  on the slip plane and total dislocation density is

$$\tau = CGb \sqrt{\rho_S + \rho_G} \quad (4.1)$$

where, as before,  $G$  is the shear modulus,  $b$  is the magnitude of the Burger's vector and  $C$  is a constant taken to be 0.3 by Ashby [5]. The contribution to flow stress from the Peierls-Nabarro or lattice-friction stress has been dropped from (4.1), as we shall focus on applications where strain hardening dominates the response. Other couplings between  $\rho_S$  and  $\rho_G$  are possible; equation (4.1) gives one particular form of non-linear interaction between flow stress  $\tau$  and dislocation densities  $\rho_S$  and  $\rho_G$ . We shall subsequently modify this functional relationship in order to develop a phenomenological theory which fits within the well-established general framework of plasticity theory.

In order to define  $\rho_G$  precisely for the case of a single slip system we assume that slip occurs in a direction  $\mathbf{s}$  aligned with the  $x_1$  axis, and the normal to the slip plane is along the  $x_2$  axis as shown in Fig. 4(a). Thus the Burger's vector  $\mathbf{b}$  of dislocations inducing the slip is codirectional with  $\mathbf{s}$ . A gradient of slip  $\partial\gamma/\partial x_1$  gives rise to a density

$$\frac{1}{b} \frac{\partial\gamma}{\partial x_1}$$

of geometrically necessary edge dislocations lying along the  $x_3$  direction. Likewise, a gradient of slip  $\partial\gamma/\partial x_3$  gives rise to a density  $(1/b)(\partial\gamma/\partial x_3)$  of screw dislocations lying along the  $x_1$  direction. As shown in Fig. 3, a slip gradient in the  $\mathbf{m}$  direction involves no storage of dislocations.

#### 4.2. A continuum measure of geometrically necessary dislocations

Now consider the case of a polycrystal containing many slip systems. The appropriate measure of the density of geometrically necessary dislocations is Nye's dislocation density tensor  $\alpha$ , defined by equation (3.5). Note that  $\alpha$  can only be defined with reference to specified slip systems. For the purposes of developing a phenomenological isotropic theory freed from the context of a crystal lattice an alternative approximate measure of dislocation density is proposed.

Split the usual strain measure  $\epsilon_{ij} \equiv \frac{1}{2}(u_{i,j} + u_{j,i})$  into elastic and plastic parts,  $\epsilon_{ij}^e$  and  $\epsilon_{ij}^p$ , respectively. The symmetric part of  $\gamma_{ij}$  in (3.2) is the plastic strain  $\epsilon_{ij}^p$ , that is

$$\epsilon_{ij}^p \equiv \frac{1}{2}(\gamma_{ij} + \gamma_{ji}). \quad (4.2)$$

Now introduce the curvature tensor  $\chi$ , defined by

$$\chi_{ni} \equiv \theta_{n,i} = \frac{1}{2}e_{njk}u_{k,ji} = e_{nkj}\epsilon_{ij,k} \quad (4.3)$$

where  $\theta_n \equiv \frac{1}{2}e_{njk}u_{k,j}$  is the rotation vector associated with a displacement field  $u_i$ . Since the divergence of  $\theta$  vanishes  $\chi_{kk} = 0$ . Also note that in general  $\chi_{ij} \neq \chi_{ji}$ . Decompose  $\chi$  into its elastic and plastic parts,  $\chi = \chi^{el} + \chi^{pl}$  where

$$\chi_{ni}^{el} = e_{nkj}\epsilon_{ij,k}^{el} \quad (4.4a)$$

and

$$\chi_{ni}^{pl} = e_{nkj}\epsilon_{ij,k}^{pl}. \quad (4.4b)$$

Note that  $\chi^{pl}$  is related to  $\epsilon^{pl}$  in an analogous manner to the relationship between  $\alpha$  and  $\gamma$ . The tensor  $\chi^{pl}$  will be used here as an approximate measure of the density of geometrically necessary dislocations. It remains a meaningful quantity when no crystal structure is embedded in the material since it is defined in terms of a plastic strain  $\epsilon^{pl}$  and not the slip tensor  $\gamma$ .

The magnitude of  $\chi^{pl}$  will be used as the scalar measure of the density of geometrically necessary dislocations. Thus, with a magnitude definition

$$\chi_e = \sqrt{\frac{2}{3}\chi_{ij}^{pl}\chi_{ij}^{pl}} \quad (4.5)$$

we take the density of geometrically necessary dislocations to be

$$\rho_G = \frac{\chi_e}{b}. \quad (4.6)$$

A scale factor of order unity is of no concern in (4.6) since it will be absorbed in the length scale  $l$  introduced later. In this simplest generalization of  $J_2$ -deformation theory, the role of the other invariants of  $\chi^{pl}$  is not considered. Note that  $\chi_e$  is related to  $\chi^{pl}$  in the same manner that the effective plastic strain  $\epsilon_e$  is related to the plastic strain  $\epsilon^{pl}$

$$\epsilon_e = \sqrt{\frac{2}{3}\epsilon_{ij}^{pl}\epsilon_{ij}^{pl}}. \quad (4.7)$$

In a similar manner, an appropriate measure of the density of statistically stored dislocations is

$$\rho_s = \frac{\epsilon_e}{\lambda_I b} \quad (4.8)$$

in stage I, and

$$\rho_s = \frac{\epsilon_e^2}{\lambda_{II} b} \quad (4.9)$$

in stage II, where  $\lambda_I$  and  $\lambda_{II}$  are fixed slip distances of the order of  $\lambda_I = 1$  mm in stage I and  $\lambda_{II} = 10$   $\mu$ m in stage II, as can be inferred from the data for copper shown in Fig. 2. It is thought that these numerical values for  $\lambda_I$  and  $\lambda_{II}$  are correct to within an order of magnitude for other f.c.c. metals in addition to copper.

#### 5. A CANDIDATE STRAIN GRADIENT PLASTICITY LAW

The above considerations lead naturally to a phenomenological theory in which material hardening is dependent upon both  $\epsilon^{pl}$  and  $\chi^{pl}$ . A linear elasticity theory in terms of  $\epsilon$  and  $\chi$  has been developed by Toupin [20], Mindlin and Tiersten [21] and Koiter [22]. This couple stress theory is summarized in Appendix B. We extend their theory to a deformation theory version of plasticity. In a deformation theory there is no formal distinction between the elastic and plastic components of displacement and of strain, and we write  $\epsilon_e = \sqrt{\frac{2}{3}}\epsilon_{ij}\epsilon_{ij}$  and  $\chi_e = \sqrt{\frac{2}{3}}\chi_{ij}\chi_{ij}$ . The work conjugates of  $\epsilon$  and  $\chi$  are the symmetric Cauchy stress tensor  $\sigma$  and the couple stress tensor  $\mu$ . Following Koiter [22], and as emphasized in Appendix B, we may legitimately assume that  $\mu_{kk} = 0$ . Thus the deviatoric couple stress tensor  $m$  equals the couple stress tensor  $\mu$ . The solid is also taken to be incompressible. On equating the incremental work of deformation to the increase in elastic stored energy  $w$  we get

$$\delta w = \sigma_{ij}\delta\epsilon_{ij} + \mu_{ij}\delta\chi_{ji} = s_{ij}\delta\epsilon_{ij} + m_{ij}\delta\chi_{ji} \quad (5.1)$$

where  $s$  is the deviatoric part of the symmetric stress tensor  $\sigma$ .

Consider again a polycrystal containing both statistically stored and geometrically necessary dislocations. Motivated by equations (4.1) and (4.7)–(4.9), we postulate that the strain energy density function  $w$  depends only upon  $\epsilon_e$  and  $\chi_e$ . In particular, it is mathematically convenient to assume that  $w$  depends only upon the single scalar strain measure  $\mathcal{E}$ , where

$$\mathcal{E}^2 \equiv \epsilon_e^2 + l^2\chi_e^2. \quad (5.2)$$

The length scale  $l$  is a material length scale, and is required on dimensional grounds. When the strain field  $\epsilon$  in the polycrystal varies over a length scale on the order of or less than  $l$ , strain gradient effects become significant. An effective stress measure  $\Sigma$  which is the work conjugate to  $\mathcal{E}$  is defined by

$$\Sigma = \frac{dw(\mathcal{E})}{d\mathcal{E}} \quad (5.3)$$



The stress measure  $\Sigma$  is a unique function of the strain measure  $\mathcal{E}$ , and vice versa.

The symmetric components  $s_{ij}$  of the deviatoric stress tensor and the deviatoric components  $m_{ij}$  of the couple stress tensor follow from (5.1) and (5.2) as

$$s_{ij} = \frac{\partial w}{\partial \epsilon_{ij}} = \Sigma \frac{\partial \mathcal{E}}{\partial \epsilon_{ij}} = \frac{2}{3} \frac{\Sigma}{\mathcal{E}} \epsilon_{ij} \quad (5.4a)$$

and

$$m_{ij} = \frac{\partial w}{\partial \chi_{ji}} = \Sigma \frac{\partial \mathcal{E}}{\partial \chi_{ji}} = \frac{2}{3} l^2 \frac{\Sigma}{\mathcal{E}} \chi_{ji}. \quad (5.4b)$$

Substitution of (5.4a) into the relation  $\epsilon_e^2 = \frac{2}{3} \epsilon_{ij} \epsilon_{ij}$ , and (5.4b) into the relation  $\chi_e^2 = \frac{2}{3} \chi_{ij} \chi_{ij}$  gives, via (5.2)

$$\Sigma^2 = \sigma_e^2 + l^{-2} m_e^2 \quad (5.5a)$$

where

$$\sigma_e \equiv \sqrt{\frac{3}{2} s_{ij} s_{ij}} \quad (5.5b)$$

and

$$m_e \equiv \sqrt{\frac{3}{2} m_{ij} m_{ij}}. \quad (5.5c)$$

The effective stress  $\sigma_e$  and effective couple stress  $m_e$  are the work conjugates to  $\epsilon_e$  and  $\chi_e$  in the sense that  $dw = \sigma_e d\epsilon_e + m_e d\chi_e$ .

For the purpose of some specific calculations in the following section we shall adopt a simple power law relationship between  $\Sigma$  and  $\mathcal{E}$

$$\Sigma = \Sigma_0 \mathcal{E}^N = \Sigma_0 (\epsilon_e^2 + l^2 \chi_e^2)^{N/2}. \quad (5.6)$$

It is instructive to compare (5.6) with the constitutive law suggested by dislocation theory. Upon substituting (4.6), and (4.8) or (4.9) into (4.1) we find

$$\tau = CG \sqrt{(b\epsilon_e/\lambda_I) + b\chi_e} \quad (5.7a)$$

for stage I behavior and

$$\tau = CG \sqrt{(b\epsilon_e^2/\lambda_{II}) + b\chi_e} \quad (5.7b)$$

for stage II behavior. If instead of taking the arithmetic mean  $\frac{1}{2}(\rho_S + \rho_G)$  of the dislocation densities in (4.1), we adopt the harmonic mean  $\frac{1}{2}\sqrt{\rho_S^2 + \rho_G^2}$ , then (5.6a) and (5.6b) are replaced by

$$\tau = CG[(b\epsilon_e/\lambda_I)^2 + b^2\chi_e^2]^{1/4} \quad (5.7c)$$

and

$$\tau = CG[(b\epsilon_e^2/\lambda_{II})^2 + b^2\chi_e^2]^{1/4}. \quad (5.7d)$$

Equation (5.6) most closely mimics the relation (5.7c). The exact form of the coupling between hardening due to statistically stored dislocations and geometrically necessary dislocations is not known. Here, we adopt a pragmatic approach, exploiting the nice mathematical consequences which follow from the assumed form, and take (5.6) as representative of the coupling between strain hardening and strain gradient hardening. In the limit of  $l\chi_e \ll \epsilon_e$ , strain gradients become insignificant and strain hardening is due only to statistically stored dislocations. Then the above relations reduce to their counterparts for a conventional power law  $J_2$ -deformation theory solid.

At the other extreme, strain gradients dominate; then, the geometrically necessary dislocations overwhelm the statistically stored dislocations, and on taking  $N = 1/2$  equation (5.6) reduces to all of the versions in (5.7).

## 6. TORSION OF A CIRCULAR CYLINDRICAL BAR

We consider torsion of a circular cylindrical bar as an example of the application of the strain gradient theory introduced above. The analysis is used in the following section to interpret the results from experiments on thin copper wires.

We take the  $x_3$  axis of a Cartesian co-ordinate system  $(x_1, x_2, x_3)$  to lie along the axis of the bar. For later convenience, a cylindrical polar co-ordinate system  $(r, \theta, x_3)$  is also introduced, as shown in the insert of Fig. 9 with the radius of the bar as  $a$ . Let  $\kappa$  be the twist per unit length of the bar, taken to be positive without loss of generality. Start by assuming the same displacement field as in classical torsion

$$u_1 = -\kappa x_2 x_3 \quad u_2 = \kappa x_1 x_3 \quad u_3 = 0. \quad (6.1)$$

The associated non-vanishing components of strain  $\epsilon_{ij}$  are

$$\epsilon_{13} = \epsilon_{31} = -\frac{1}{2} \kappa x_2 \quad \epsilon_{23} = \epsilon_{32} = \frac{1}{2} \kappa x_1 \quad (6.2)$$

and the non-vanishing components of the curvature tensor  $\chi$  are

$$\chi_{11} = \chi_{22} = -\frac{1}{2} \kappa \quad \chi_{33} = \kappa. \quad (6.3)$$

Values for the effective curvature  $\chi_e \equiv \sqrt{\frac{2}{3} \chi_{ij} \chi_{ij}} = \kappa$ , effective strain  $\epsilon_e \equiv \sqrt{\frac{2}{3} \epsilon_{ij} \epsilon_{ij}} = (1/\sqrt{3}) \kappa r$ , and strain measure  $\mathcal{E} \equiv \sqrt{\epsilon_e^2 + l^2 \chi_e^2} = \kappa \sqrt{\frac{1}{3} r^2 + l^2}$  follow directly from (6.2) and (6.3). We assume that the stress measure  $\Sigma$  is related to  $\mathcal{E}$  via (5.6).

The non-vanishing components of the deviatoric couple stress tensor are, via (5.4b) and (5.6)

$$m_{11} = m_{22} = -\frac{1}{3} \Sigma_0 \mathcal{E}^{N-1} l^2 \kappa \quad m_{33} = \frac{2}{3} \Sigma_0 \mathcal{E}^{N-1} l^2 \kappa. \quad (6.4)$$

The mean stress  $\frac{1}{3} \sigma_{kk}$  vanishes, and the non-vanishing components of the symmetric stress tensor are, via (5.4a)

$$\begin{aligned} \sigma_{13} = \sigma_{31} &= -\frac{1}{3} \Sigma_0 \mathcal{E}^{N-1} \kappa x_2 \\ \sigma_{23} = \sigma_{32} &= \frac{1}{3} \Sigma_0 \mathcal{E}^{N-1} \kappa x_1. \end{aligned} \quad (6.5)$$

The anti-symmetric components  $\tau_{ij}$  of the stress tensor follow from the equilibrium relation [see Appendix, equation (B10)]

$$\tau_{23} = -\frac{1}{2} m_{11,1} = -\frac{(1-N)}{18} \Sigma_0 l^2 \kappa^3 \mathcal{E}^{N-3} x_1 \quad (6.6a)$$

and

$$\tau_{13} = \frac{1}{2} m_{22,2} = \frac{(1-N)}{18} \Sigma_0 l^2 \kappa^3 \mathcal{E}^{N-3} x_2. \quad (6.6b)$$

The fundamental equations of equilibrium (B9) are satisfied by the above solution. The boundary tractions  $\bar{T}_i$  and  $\bar{q}_i$  also vanish on the cylindrical surface

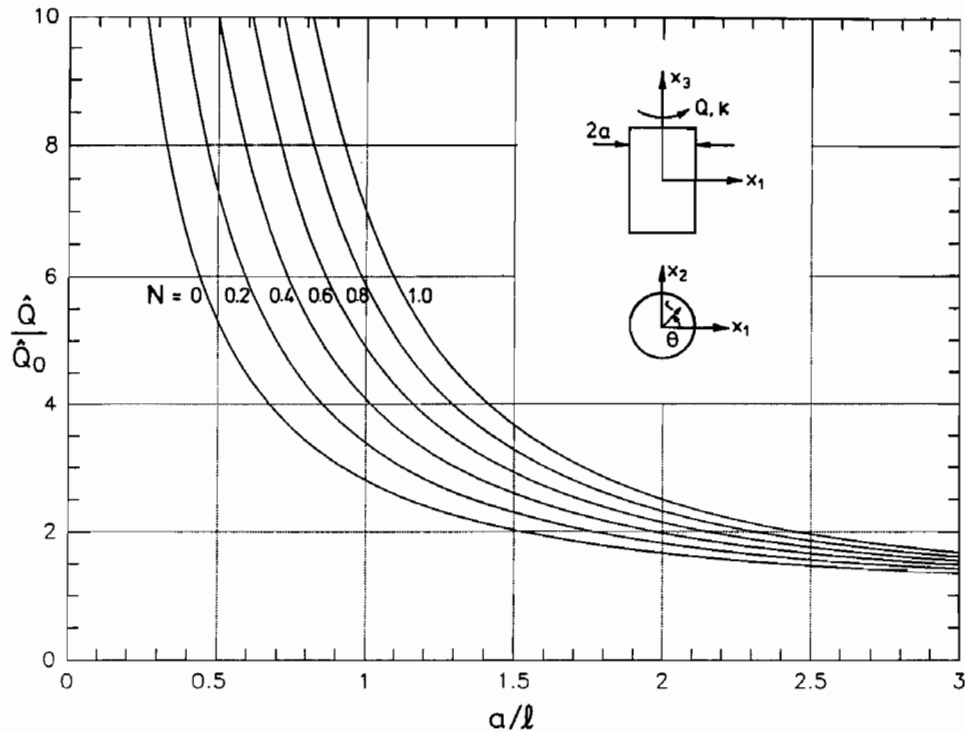


Fig. 9. Effect of non-dimensionalized bar radius  $a/l$  and strain hardening index  $N$  upon the torsional rigidity of a circular bar.

of the bar, by (B16) and (B17). Hence the displacement field (6.1) satisfies all requirements.

The relation between the torque  $Q$  and the twist per unit length  $\kappa$  is deduced most simply by noting that the strain energy for a unit length of the bar is given by

$$\int_V w(\mathcal{E}) dV = \int_V \left( \int_0^{\mathcal{E}} \Sigma(\mathcal{E}) d\mathcal{E} \right) dV = \int_0^{\kappa} Q(\kappa) d\kappa. \quad (6.7)$$

Since  $\Sigma$  and  $Q$  are homogeneous and of degree  $N$  in  $\mathcal{E}$  and  $\kappa$ , respectively, we may re-write (6.7) as

$$\int_V w(\mathcal{E}) dV = \int_V \frac{\Sigma \mathcal{E}}{N+1} dV = \frac{Q\kappa}{N+1}. \quad (6.8)$$

Now substitute for  $\mathcal{E} = \kappa \sqrt{\frac{1}{3}r^2 + l^2}$  and for  $\Sigma = \Sigma_0 \mathcal{E}^N$  into (6.8), and integrate over the volume to get

$$Q = \frac{6\pi}{N+3} \Sigma_0 \kappa^N \left[ \left( \frac{1}{3}a^2 + l^2 \right)^{(N+3)/2} - l^{N+3} \right]. \quad (6.9)$$

The formula (6.9) may be derived alternatively by integration of the stress tractions and couple stress tractions over the surface of the bar.

The torque may be re-written in the non-dimensional form  $\hat{Q}$ , where

$$\hat{Q} \equiv \frac{Q}{\Sigma_0 a^3 (\kappa a)^N} = \frac{6\pi}{N+3} \left[ \left[ \frac{1}{3} + \left( \frac{l}{a} \right)^2 \right]^{(N+3)/2} - \left( \frac{l}{a} \right)^{N+3} \right]. \quad (6.10)$$

Evidently, the non-dimensional torque  $\hat{Q}$  is a function only of  $l/a$  and  $N$ . In the limit of  $l=0$  couple

stresses vanish and the non-dimensional torque, designated by  $\hat{Q}_0$  is

$$\hat{Q}_0 \equiv \frac{Q(l=0)}{\Sigma_0 a^3 (\kappa a)^N} = \frac{2\pi}{(N+3)(\sqrt{3})^{N+1}}. \quad (6.11)$$

The significance of couple stresses upon influencing the torque carried by the bar may be gauged from a plot of  $\hat{Q}/\hat{Q}_0$  vs  $a/l$  for  $0 \leq N \leq 1$ , see Fig. 9. It is clear from the figure that  $\hat{Q}/\hat{Q}_0$  increases with decreasing  $a/l$  and with increasing  $N$ . For a bar of radius  $a$  equal to the microstructural length scale  $l$  the ratio  $\hat{Q}/\hat{Q}_0$  equals 2.804 for  $N=0$ , and equals 7 for  $N=1$ . The strain gradient effect dominates the response for  $a/l < 1$ , and has a mild influence for  $a/l > 3$ . For large  $a/l$ ,  $\hat{Q}/\hat{Q}_0$  is given asymptotically by

$$\frac{\hat{Q}}{\hat{Q}_0} = 1 + \frac{3}{2}(N+3) \left( \frac{l}{a} \right)^2 + O \left( \frac{l}{a} \right)^{N+3}. \quad (6.12)$$

This formula shows that the strain gradient effect diminishes rapidly with increasing  $a/l$  for large  $a/l$ .

## 7. COMPARISON WITH EXPERIMENT

The experiments clearly demonstrate an influence of wire diameter on torsional hardening, an effect not observed in the tensile tests. We have attributed this to an added, geometrically necessary component of the dislocation density stored during deformation. The relevance of texture has not been investigated in this study. Further work is needed to elucidate the degree to which texture might influence the results.

We fit the predicted  $Q/a^3$  vs  $\kappa a$  response (6.10) to the experimental data in order to deduce a value for the microstructural length scale  $l$ . (It is realized that the torsion tests were carried out to large strains and that the theory of the previous section is a small strain theory.) In order to estimate  $l$ , the following procedure is adopted.

For each diameter of wire we record from Fig. 6 the value of  $Q/a^3$  at  $\kappa a = 0.3$ . A useful measure of the degree of strain gradient strengthening associated with each diameter of wire is the ratio  $R \equiv (Q/a^3) / (Q/a^3)_{2a=170\mu\text{m}}$  where  $Q/a^3$  (measured at  $\kappa a = 0.3$ ) is for a wire of diameter  $2a$ , and  $(Q/a^3)_{2a=170\mu\text{m}}$  (also measured at  $\kappa a = 0.3$ ) is for the wire of diameter  $2a = 170\mu\text{m}$ . Note from equation (6.10) that

$$R = \frac{Q/a^3}{(Q/a^3)_{2a=170\mu\text{m}}} = \frac{\hat{Q}}{(\hat{Q})_{2a=170\mu\text{m}}} \quad (7.1)$$

The parameter  $\Sigma_0$  does not enter into the ratio  $R$ . Predicted values of the ratio  $R = \hat{Q}/(\hat{Q})_{2a=170\mu\text{m}}$  are evaluated from (6.10) and plotted in Fig. 10 as a function of  $l$  for the wire diameters  $2a = 12\text{--}30\mu\text{m}$ . We use these theoretical curves to estimate values for  $l$  from the observed values of  $R$ . The estimated values for  $l$  are shown for each wire diameter by the arrows in Fig. 10. We find that  $l$  is in the range  $2.6\text{--}5.1\mu\text{m}$ , with a mean value of  $3.7\mu\text{m}$ . This is of the expected order of magnitude, and is in rough agreement with

the value  $\lambda_{II} = 10\mu\text{m}$  at a shear strain of 0.3, measured by Mader [25].

8. CONCLUDING DISCUSSION

In this paper we have developed a phenomenological plasticity law whereby the stress is a function of both strain and strain gradient. Several observed plasticity phenomena display a size effect such that the greater is the imposed strain gradient the greater is the degree of hardening. For example, hardness, when measured on a micron scale, is greater than that at the millimeter scale; a few volume percent of micron scale non-deforming particles dramatically raises the rate of work hardening in metals, those of millimeter scale do not; and, as we have shown here, wires with diameters of a few tens of microns work harden, when twisted, faster than those of millimeter diameter.

In addition to elucidating these scale-dependent phenomena, a strain gradient plasticity theory has other potential applications. One is that of developing a fuller understanding of crack tip plasticity, where gradients are particularly strong. Another is the modelling of shear bands. As is well appreciated, the thickness of a shear band must be related to an internal length scale.

The theory of geometrically necessary dislocations introduced by Ashby [5, 6] and developed further in

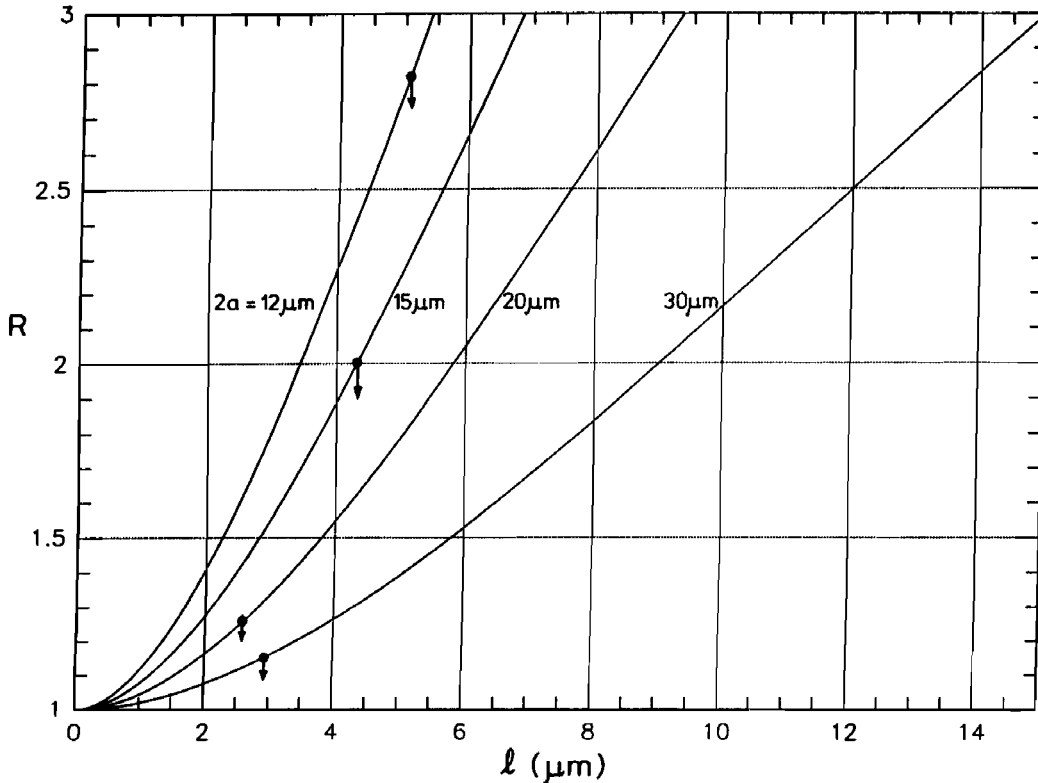


Fig. 10. Non-dimensional torque vs microstructural length  $l$  predicted by the phenomenological plasticity law. The arrows show the experimental data used to estimate the value of  $l$  for copper.

the current paper suggests that strengthening is associated with a first order gradient in plastic strain. There appears to be little reason to consider higher order strain gradients when considering low temperature crystal plasticity. Zbib and Aifantis [15] assume that strain gradient strengthening is associated with the invariants  $\nabla^2 \epsilon_c$  and  $|\nabla \epsilon_c|$ . Their approach has a number of similarities with the present theory, but is based on a different variational principle [27]. In earlier papers, Muhlhaus and Aifantis [13, 14] assume instead that strengthening is associated with terms of order  $\nabla^2 \epsilon_c$  and  $\nabla^4 \epsilon_c$ ; in torsion these higher order strain gradients vanish and no size effect is predicted.

**Acknowledgements**—The authors are grateful for financial support from the U.S. Office of Naval Research, contract numbers N00014-91-J-1916 and N00014-92-J-1960. GMM was funded by D.A.A.D. The authors also wish to thank Electrisola GmbH and Co. KG, Germany, for supplying the copper wires.

#### REFERENCES

1. L. M. Brown, private communication (1993).
2. A. Kelly and R. B. Nicholson, *Prog. Mater. Sci.* **10**, 151 (1963).
3. R. Ebeling and M. F. Ashby, *Phil. Mag.* **13**, 805 (1966).
4. U. Essmann, M. Rapp and M. Wilkins, *Acta metall.* **16**, 1275 (1968).
5. M. F. Ashby, *Phil. Mag.* **21**, 399 (1970).
6. M. F. Ashby, in *Strengthening Methods in Crystals* (edited by A. Kelly and R. B. Nicholson), p. 137 (1971).
7. J. F. Nye, *Acta metall.* **1**, 153 (1953).
8. A. H. Cottrell, *The Mechanical Properties of Matter*, p. 277. Wiley, New York (1964).
9. K. C. Russel and M. F. Ashby, *Acta metall.* **18**, 891 (1970).
10. L. M. Brown and W. M. Stobbs, *Phil. Mag.* **34**, 351 (1976).
11. S. J. Basinski and Z. S. Basinski, in *Recrystallization, Grain Growth and Textures*, p. 26. Am. Soc. Metals, Metals Park, Ohio (1966).
12. E. C. Aifantis, *Int. J. Plasticity* **3**, 211 (1987).
13. H. B. Muhlhaus and E. C. Aifantis, *Int. J. Solids Struct.* **28**, 845 (1991).
14. H. B. Muhlhaus and E. C. Aifantis, *Acta mechanica* **89**, 217 (1991).
15. H. M. Zbib and E. C. Aifantis, *Acta mechanica* **92**, 209 (1992).
16. E. Kroner, *Kontinuumstheorie der versetzungen und eigenspannungen*. Springer, Berlin (1958).
17. E. Kroner, *Physica status solidi* **1**, 3 (1961).
18. E. Kroner, *Appl. Mech. Rev.* **15**(8), 599 (1962).
19. R. Hill and J. R. Rice, *J. Mech. Phys. Solids* **20**, 401 (1972).
20. R. A. Toupin, *Arch. Rat. Mech. Anal.* **11**, 385 (1962).
21. R. D. Mindlin and H. F. Tiersten, *Arch. Rat. Mech. Anal.* **11**, 415 (1962).
22. W. T. Koiter, *Proc. Ned. Akad. Wet. (B)* **67**, 17 (1964).
23. E. and F. Cosserat, *Theorie des corps deformables*. Herman, Paris (1909).
24. R. D. Mindlin, *Arch. Rat. Mech. Anal.* **16**, 51 (1964).
25. R. D. Mindlin, *J. Solids Struct.* **1**, 417 (1965).
26. S. Mader, *Z. Physik* **149**, 73 (1957).
27. H. M. Zbib, private communication (1993).

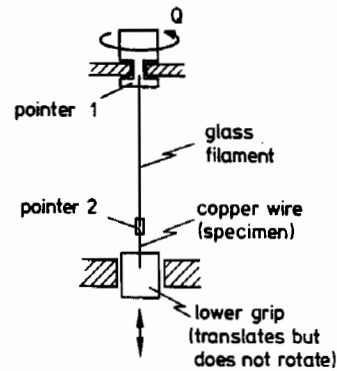


Fig. A1. Schematic of torsion test rig.

#### APPENDIX A

##### Apparatus for Tension and Torsion Tests

The tension tests were performed on a 50 mm gauge length of copper wire, using a conventional screw driven test machine and a specially designed sensitive load cell. The load cell consisted of a 0.5 mm thick cantilever beam of rectangular section; it was loaded transversely at its free end by the copper wire. Strain gauges were placed near the built-in end of the beam and were used to detect the load on the copper wire.

The torsion tests were performed using a specially designed screw driven torsion machine sketched in Fig. A1. The bottom end of the copper wire specimen (of gauge length 2 mm) was glued to a lower grip, and the top end to a 60 mm long glass filament; the glass filament acted as a torsional load cell. The free end of the glass filament was twisted using a gear drive train and electric motor. The twist along the length of the glass filament was measured by two needle pointers and protractors, and gave a measure of the torque. Calibration of the glass filament load cell was carried out separately using a dead weight and pulley arrangement. The torsional strength of the copper wires roughly scales with diameter to the third power: to maximize sensitivity of the torsional load cell glass filaments were used of diameter in the range 55–250  $\mu\text{m}$ .

The relative twist of the two ends of the copper wire was measured by the needle pointer attached to the top end of the wire (the other end was fixed to the lower grip of the test machine which could translate but not rotate). During a test the wire elongated by a few percent, causing the glass filament to bow. This was corrected for by translating the lower grip of the test machine via a gear drive.

#### APPENDIX B

##### Couple Stress Theory

The Cosserat theory [23] of couple stresses in elasticity was further developed in the early 1960's notably by Toupin [20], Mindlin and Tiersten [21], Mindlin [24, 25] and Koiter [22]. Here, the main results are summarized and the development closely follows the lucid account given by Koiter [22]. The classical theory of elasticity (neglecting couple stresses) assumes that the transmission of loads on both sides of an infinitesimal surface element  $dS$  within the material is described completely by a force vector  $T dS$  acting on the surface element. In couple stress theory it is assumed that a surface element  $dS$  may transmit both a force vector  $T dS$  and a couple vector  $q dS$ .

We consider an arbitrary volume  $V$  of the body bounded by a piecewise smooth surface  $S$ . Equilibrium of forces on the body gives

$$\int_S T dS = 0 \quad (\text{B1})$$

and equilibrium of moments gives

$$\int_S (\mathbf{r} \times \mathbf{T} + \mathbf{q}) dS = 0 \quad (\text{B2})$$

where  $\mathbf{r}$  is the radius vector from an arbitrary fixed point, and body forces and body couples have been neglected.

Now introduce Cartesian co-ordinates  $x_i$  with the origin at this fixed point. Let  $\sigma_{ij}$  and  $\tau_{ij}$  be the symmetric and anti-symmetric parts of the Cauchy stress tensor, respectively. Then  $(\sigma_{ij} + \tau_{ij})$  denote the components of  $T_j$  on a plane with a unit normal  $n_i$

$$T_j = (\sigma_{ij} + \tau_{ij})n_i. \quad (\text{B3})$$

Similarly, let  $\mu_{ij}$  denote the components of  $q_j$  on a plane with a unit normal  $n_i$

$$q_j = \mu_{ij}n_i. \quad (\text{B4})$$

We refer to  $\boldsymbol{\mu}$  as the couple stress tensor.

Application of the divergence theorem to (B1) and (B2), using (B3) and (B4), gives the usual force equilibrium equation

$$\sigma_{\mu,j} + \tau_{\mu,j} = 0 \quad (\text{B5})$$

and the moment equilibrium equation

$$e_{ijk}\tau_{jk} + \mu_{\mu,j} = 0. \quad (\text{B6})$$

It is convenient to split  $\boldsymbol{\mu}$  into its spherical part,  $\mu$

$$\mu \equiv \frac{1}{3}\mu_{kk} \quad (\text{B7})$$

and its deviatoric part,  $\mathbf{m}$

$$m_{ij} = \mu_{ij} - \mu\delta_{ij}. \quad (\text{B8})$$

Equations (B5–B8) may be combined to give a single triple of final equations of equilibrium

$$\sigma_{mn,m} - \frac{1}{2}e_{mnn}m_{ji,jm} = 0. \quad (\text{B9})$$

The anti-symmetric part of the stress tensor  $\boldsymbol{\tau}$  may be expressed in terms of  $\boldsymbol{\mu}$  by rearranging (B6) to the form

$$\tau_{mn} = -\frac{1}{2}e_{imn}\mu_{\mu,j}. \quad (\text{B10})$$

#### Principle of virtual work

The principle of virtual work is conveniently formulated in terms of virtual velocities. Let  $\dot{u}_i$  denote the Cartesian components of a continuously differentiable virtual velocity field. The angular velocity vector  $\dot{\theta}_i$  has the components

$$\dot{\theta}_i = \frac{1}{2}e_{ijk}\dot{u}_{k,j}. \quad (\text{B11})$$

Denoting the rate at which work is absorbed internally per unit volume by  $\dot{w}$ , the equation of virtual work reads

$$\int_V \dot{w} dV = \int_S T_i \dot{u}_i + q_i \dot{\theta}_i dS \quad (\text{B12})$$

where the volume  $V$  is contained within the closed surface

$S$ . Using the divergence theorem, the right hand side of (B12) may be re-arranged to the form

$$\int_S T_i \dot{u}_i + q_i \dot{\theta}_i dS = \int_V (\sigma_{\mu,j} + \tau_{\mu,j})\dot{u}_i + (e_{ijk}\tau_{jk} + \mu_{\mu,j})\dot{\theta}_i + (\sigma_{ij} + \tau_{ij})\dot{\epsilon}_{ij} + \mu_{ij}\dot{\chi}_{ji} dV \quad (\text{B13})$$

where the strain tensor  $\epsilon_{ij} \equiv \frac{1}{2}(u_{i,j} + u_{j,i})$ , and the curvature tensor  $\chi_{ij} \equiv \theta_{i,j}$ . Consider the right hand side of (B13). The first term vanishes by force equilibrium (B5), and the second term vanishes by moment equilibrium (B6). Since the strain tensor is symmetric, we have  $(\sigma_{ij} + \tau_{ij})\dot{\epsilon}_{ij} = \sigma_{ij}\dot{\epsilon}_{ij}$ ; the curvature tensor is deviatoric in nature, and so  $\mu_{ij}\dot{\chi}_{ji} = m_{ij}\dot{\chi}_{ji}$ . Thus, (B13) reduces to

$$\int_S T_i \dot{u}_i + q_i \dot{\theta}_i dS = \int_V \sigma_{ij}\dot{\epsilon}_{ij} + m_{ij}\dot{\chi}_{ji} dV. \quad (\text{B14})$$

Now consider the left hand side of (B14). If  $\dot{u}_i$  is specified on the surface  $S$ , the normal component of  $\dot{\theta}_i$  cannot be prescribed independently. The two tangential components of  $\dot{\theta}_i$  may be specified, giving a total of five kinematic boundary conditions. This implies that at any point of a smooth part of the surface we may specify *three* reduced stress tractions  $\bar{T}_i$ , and *two* reduced couple stress tractions  $\bar{q}_i$  which are tangential to the surface. The rate of work of surface tractions may be rewritten

$$\int_S T_i \dot{u}_i + q_i \dot{\theta}_i dS = \int_S \bar{T}_i \dot{u}_i + \bar{q}_i \dot{\theta}_i dS + \sum_{\alpha} \oint_{C_{\alpha}} \bar{Q} \dot{u}_i dt \quad (\text{B15})$$

where

$$\begin{aligned} \bar{T}_i &\equiv T_i - \frac{1}{2}e_{kki}(q_j n_j)_{,k} n_h \\ &= \sigma_n n_h + \frac{1}{2}e_{hki} n_h [m_{jk,j} - (m_{rs} n_r n_s)_{,k}] \end{aligned} \quad (\text{B16})$$

and

$$\bar{q}_i \equiv q_i - q_j n_j n_i = m_{ji} n_j - (m_{rs} n_r n_s) n_i. \quad (\text{B17})$$

The last term on the right hand side of (B15) requires further explanation. The piecewise smooth surface can be divided into a finite number of smooth parts  $S_{\alpha}$  each bounded by an edge  $C_{\alpha}$ . Integration is conducted along the arc length  $l$  of each edge  $C_{\alpha}$  in the direction  $\mathbf{t}$  of the edge. The measure  $\bar{Q}$  may be viewed as a line load per unit length of edge, and equals half of the difference  $(q_i n_i)_{+} - (q_i n_i)_{-}$  of the normal component of the couple traction at each side of the edge. Thus

$$\bar{Q} = \frac{1}{2}(q_i n_i)_{+} - \frac{1}{2}(q_i n_i)_{-} = \frac{1}{2}(m_{ij} n_i n_j)_{+} - \frac{1}{2}(m_{ij} n_i n_j)_{-}. \quad (\text{B18})$$

We note that the first invariant  $3\mu$  of the couple stress tensor does not appear in the basic equations of equilibrium (B9), the virtual work equation (B14) or the boundary conditions (B16–B18). Thus,  $\mu$  is indeterminate in the theory, and without any loss of generality we may put  $\mu \equiv 0$ ; then,  $m_{ij} \equiv \mu_{ij}$ .

